Feasibility and Fundamental Limits of Energy-Harvesting Based M2M Communications

Noname manuscript No.
(will be inserted by the editor)

Feasibility and Fundamental Limits of Energy-Harvesting Based M2M Communications

Jukka Rinne · Jari Keskinen · Paul R. Berger · Donald Lupo · Mikko Valkama

Received: date / Accepted: date

Abstract Energy-efficient, reliable and scalable machine-to-machine (M2M) communications is the key technical enabler of Internet-of-Things (IoT) networks. Furthermore, as the number of populated devices is constantly increasing, self-sustaining or energy-autonomous IoT nodes are a promising prospect receiving increasing interest. In this paper, the feasibility and fundamental limits of energy harvesting based M2M communication systems are studied and presented. The derived theoretical bounds are effectively based on the Shannon theorem, combined with selected propagation loss models, assumed link nonidealities, as well as the given energy harvesting and storage capabilities. Fundamental limits and available operational time of the communicating nodes are derived and analyzed, together with extensive numerical results evaluated in different practical scenarios for low power sensor type communication applications.

Keywords M2M communications · Shannon limit · propagation loss · energy harvesting · supercapacitor · available operational time

1 Introduction

It has been recently forecast, e.g. in [2], that there will be around 29 billion connected devices by 2022, of which around 18 billion will be related to IoT. These connected devices should all operate and integrate smoothly

This is an extended version of the earlier published paper by Rinne *et al.* [1], presented in IEEE PIMRC 2016.
This work was financially supported by the Finnish Funding Agency for Technology and Innovation (Tekes), under the project PAUL.

J. Rinne
Lab. of Electronics and Communications Engineering, Tampere University of Technology, Tampere, Finland
E-mail: jukka.rinne@tut.fi

with the Internet, while providing a vast spectrum of services in, e.g., healthcare, smart homes, industry automation, and environmental monitoring. This trend, commonly referred to as the Internet-of-Things (IoT) or Internet-of-Everything (IoE), imposes enormous challenges and requirements on the radio connectivity, in the form of machine-to-machine (M2M) communications, from coverage, energy-efficiency and scalability points of view [3]. Another closely related field is low-energy sensor networks and energy-harvesting, where the sensor and communication nodes are autonomously extracting or harvesting energy from their surroundings [4], [5].

In general, energy-autonomous M2M communications with fairly low bitrates but massive numbers of devices pose substantial demands on the component, circuit, and system designs. As the technological challenges include low power consumption of the devices [6], also the methods for obtaining or harvesting energy efficiently from different sources, as well as storing the harvested energy, are under intensive research [7]. In addition to the basic silicon/CMOS based circuits, also alternative organic/inorganic or printed electronics based solutions are raising interest [8], [9].

In this paper, the feasibility and fundamental limits of energy harvesting based machine communication systems are studied and presented. In the study, we adopt fundamental Shannon capacity laws combined with appropriate propagation loss models and assumed levels of nonidealities related to the radio link implementation, to extract fundamental performance bounds and feasibility limits for low-rate low-energy M2M communications. The study also incorporates energy harvesting issues together with the energy storage model in the form of a supercapacitor [10], [11] and selected harvesting methods. We also derive expressions for the available communication time depending on the energy harvesting and storage capabilities, combined with the targeted instantaneous communication rate and the assumed periodicity or probability to transmit or receive at a given time window. In the numerical evaluations, we specifically focus on the licence-exempt ISM bands at 433 MHz and 900 MHz (sub-1GHz) while the analysis methodology and derived expressions are valid at all other frequencies as well. The provided analysis methodology and obtained results establish clear feasibility regions and performance bounds for energy harvesting based low-rate M2M communications.

The rest of this paper is organized as follows. First, in Section 2, the fundamental channel capacity aspects are addressed and discussed. Then, in Section 3, the energy harvesting and storage issues are studied and analyzed, together with the achievable operational time for communicating at the given rate with given probabilities to transmit and receive. In Section 4, the considered path loss models are first reviewed, followed by an extensive set of numerical results. Finally, the key findings and conclusions are drawn in Section 5.

2 Fundamental Capacity Bounds

The theoretical maximum information transfer rate of any noisy channel is given by the Shannon capacity law [12]. As is very well known, this Shannon limit for communication, R, can be expressed in bits/s as

$$R = B \log_2(1 + S/N), \tag{1}$$

where B denotes the bandwidth, S refers to the received useful signal power while the noise power is denoted by N. At operational frequencies that are higher than 300 MHz, the noise is due to thermal noise [13]. In this case, the power of the noise is given by $N = kTBF$, where k, T, B, and F are the Boltzmann coefficient (1.3807×10^{-23} J/K), temperature in Kelvins, bandwidth in Hz, and noise factor in numeric form ($F = 10^{\mathrm{NF}/10}$, where NF is in decibels), respectively. The corresponding capacity in bits/s/Hz can be then expressed as

$$C = R/B = \log_2\left(1 + \frac{S}{kTBF}\right). \tag{2}$$

To make the analysis more realistic, possible implementation losses can be taken into account in (2) by introducing an additional factor μ as

$$C = \log_2\left(1 + \frac{S}{\mu kTBF}\right). \tag{3}$$

Here the implementation loss factor $\mu \geq 1$ is related to, e.g., error correcting code strength and imperfections of receiver synchronization [14]. As an example $\mu = 1.02$ (0.1 dB loss), if the coding system is tightly designed [15], while $\mu = 4$ (6 dB loss) if more relaxed operation is allowed.

Next, to express the achievable capacity as a function of the transmit power, S_{TX}, the path loss or attenuation of the propagation channel needs to be taken into account. Thus the received useful power S can be expressed as $S = S_{TX}/\lambda$, where S_{TX} is the transmitted power and λ refers to the path loss in numeric form, i.e., $\lambda = 10^{L_{\mathrm{dB}}(d)/10}$ where $L_{\mathrm{dB}}(d)$ refers to the path loss in decibels at distance d. Thus, we obtain

$$C = \log_2\left(1 + \frac{S_{TX}/\lambda}{\mu kTBF}\right). \tag{4}$$

In general, when the geographical area over which the communication may take place increases, the path loss λ increases with respect to distance, d, and hence C is decreased for given transmit power. These aspects are addressed more thoroughly later in this paper, in Section 4.

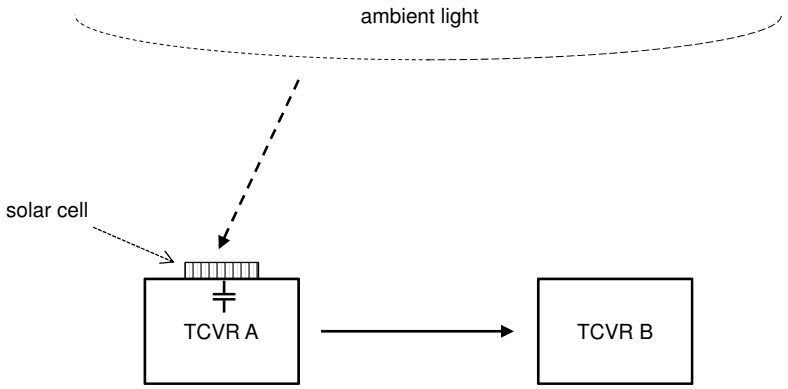

Fig. 1 Sensor system using ambient light energy (- - -) collected by solar cell and stored into supecapacitor. The communication link (—) between transceivers TCVR A and TCVR B is also shown

3 Energy Harvesting, Storage, and Achievable Operational Time

3.1 Energy Harvesting and Storage

Having the ability to harvest ambient energy in wireless devices and sensors is a very tempting prospect, compared to classical battery-only based operation [4], [5]. In general, energy can be harvested from various sources and mechanisms related to, e.g., light, movement and radio waves [16], [17]. Such energy harvesting capabilities can potentially facilitate future IoT networks with substantially enhanced self-sustainability and virtually infinite operation time, being primarily limited by the hardware constraints rather than the local energy storage.

In general, numerous different sources of ambient energy exist in the operational environment of the communicating nodes, including for example solar, indoor lighting, and thermal energy, while other good examples are vibrational, biological, chemical, and electromagnetic energy [7], [18], [19]. In addition, energy can also be harvested from various deliberately built man-made sources via wireless energy transfer.

The small amounts of energy collected by the energy harvester are continuously stored in a specific device, such as a rechargeable battery [17] or a supercapacitor as is shown in Figure 1. The energy obtained by solar cell from ambient light provides the operation of communication link between tranceivers at nodes TCVR A and TCVR B. In this paper, we consider a supercapacitor as energy storage unit due to its good cycle life compared to secondary batteries and high energy density compared to traditional capaci-

tors. In general, the maximum energy storage capability of capacitor is given by

$$E_c = \frac{1}{2} C_s U^2, \tag{5}$$

where C_s and U are the capacitance and voltage, respectively. Ideally, this energy can then be used fully for communication purposes. The constant current discharging (or charging) of a capacitor gives a linear decrease (or increase) in the capacitor potential with time [20]. In general, the usable energy is determined by the voltage level which decreases as the energy of a capacitor is used and hence the described full energy will not be available. In practice, typically a maximum of $50 \ldots 80$ percent of capacitor energy can be used due to this. Thus, we denote the useful energy by $E_u = \eta E_c$, where η refers to the fraction of useful energy relative to the maximum theoretical energy (e.g., $0.50 \ldots 0.80$).

3.2 Achievable Operational Time

Next we address the achievable operational or communication time using the available harvested energy. If the transmitter is on $100\beta_{TX}$ percent of operational time, receiver is on $100\beta_{RX}$ percent of operational time, the consumed power may be expressed as

$$P_{tcvr} = P_{TX}\beta_{TX} + P_{RX}\beta_{RX}. \tag{6}$$

Here it is supposed that the power consumption of other possible node functions are negligible and not needed to be considered in the evaluations. Besides using the energy for transmitting and receiving, part of the stored energy is lost due to the self-discharge of the supercapacitor. This can and should be taken into account when calculating the operational time by incorporating supercapacitor leakage current into the analysis. Now when the leakage current is I_l, the total consumed power is given by

$$P_{tot} = P_{tcvr} + UI_l. \tag{7}$$

When the harvested power, P_s, is greater than P_{tot}, the excessive power may be stored to supercapacitor. Thus the limiting leakage current, I_l, may be given by

$$I_l \leq (P_s - P_{tcvr})/U. \tag{8}$$

In principle, wake-up radio assisted operation [21], [22] might be applied to diminish the power consumption and hence to improve the supercapacitor usage. However due to its complexity, wake-up radio will be discarded here and hence we simply set $\beta_{RX} = 1 - \beta_{TX}$, i.e., the transmitter is on when receiver is off and vice versa, the operational time of the transceiver using fully recharged supercapacitor only, denoted here by t_{op}, can be expressed as

$$\begin{aligned} t_{op} =& E_u/P_{tot} \\ =& \eta E_c/(P_{TX}\beta_{TX} + P_{RX}(1-\beta_{TX}) + UI_l), \end{aligned} \tag{9}$$

where P_{TX} and P_{RX} are the consumed powers when in transmitter mode or in receiver mode, respectively, while E_u refers to the available energy. For later analysis, the ratio of the transmitter and receiver power consumption values is expressed by

$$\rho = P_{RX}/P_{TX}. \tag{10}$$

In general, the more complex the receiver is the more power is consumed in the receiver processing.

Furthermore, due to various processing implementation issues and finite power-efficiency, the actual transmitted power S_{TX} is always substantially smaller than the transmitter total power consumption P_{TX}. This is expressed here as

$$S_{TX} = \alpha P_{TX}, \tag{11}$$

where $\alpha \leq 1$ refers to the transmitter power efficiency. As a concrete example, α is around 0.1 in existing ZigBee transceivers [23].

3.3 Elementary Numerical Example

As a simple numerical example, we assume based on [11] that $\eta = 0.75$, $C_s = 0.5$ F, $U = 1$ V, $P_{TX} = 0.01$ mW, $\beta_{TX} = 0.01$, $\rho = 0.1$, and $I_l = 1$ μA, leading to $E_c = 0.25$ J and $E_u = 0.1875$ J. Then, based on (9), it follows that $t_{op} \approx 90000$ s (or ≈ 25 h), i.e., more than one day. Much more comprehensive numerical examples and results will be provided in Section 4, together with the explicit mapping to and dependence of the communication rates.

As discussed already earlier, various different sources may be applied to collect the required energy. As a concrete example, we consider adopting a small solar cell for this purpose. Now, to collect the amount of energy E_c with a solar cell providing harvesting power of P_s, the resulting harvesting time t_s is given by

$$t_s = E_c/P_s. \tag{12}$$

If a tight design criterion of $t_s = t_{op}$ is assumed, i.e., all the harvested power is used for transceiver operation, and adopting the values from the above example, the required P_s will be 2.79 μW. State-of-the-art solar cells will provide outdoor power intensities in the order of 100 μW/mm^2 with cost-effective amorphous cells [23]. This energy can thus be harvested by a tiny solar cell of size 0.03 mm^2 in outdoor conditions and 0.3 mm^2 in indoor conditions due to dimmer lighting. While the resulting cell sizes are very small and thus hardly even practical, this simple example clearly shows that the energy harvesting is not a limiting factor in the studied system. In practise, the energy budgeting is not as critical as assumed here, but more relaxed design criteria are used in order to allow temporal changes, e.g., in irradiance level [23]. Thus 10 percent or so larger solar cells would be needed, but this is well tolerated in the considered example case. It should be also noted, that the energy harvesting and storing operation may take place with the same time as transceiver operation. In such a case, there are no time limitations for the transceiver operation as long as

the used average power is below or equal to P_s and there is harvestable power available. Furthermore, the possible excess harvested power may be stored for later use.

4 Obtained Results and Analysis

In this section, both the capacity bounds and the available operational time are evaluated and presented considering the IEEE 802.11ah channel and propagation models, including both indoor and outdoor channel scenarios [24]. First, the path loss models of the considered use cases are shortly presented and then the corresponding capacity bounds versus the link distance, d, will be shown. Finally, the achievable operating time will be evaluated for different transmitter-receiver activity ratios. In general, we will specifically focus on the low-power, low-bandwidth applications, due to the energy-harvesting constraints.

4.1 Considered Path loss Models and Use Cases

Here, IEEE 802.11ah channel models [24] are used to model a multitude of M2M communication scenarios, incorporating outdoor with macro, outdoor pico/hotzone deployments, indoor, and outdoor Device to Device (D2D) use cases. In outdoor macro antenna height is assumed 15 m above rooftop, whereas in pico/hotzone deployments antenna is assumed at rooftop level. For outdoor D2D path loss, antenna height is assumed 1.5 m. In indoor path loss case, the model is valid for single floor scenario and the exact antenna height is left open, but can be typically in practise thought to be less than 3 m. The typical path lengths for the models are some hundreds of meters, but for macro channel even several kilometers. The path losses of these use cases at distance d in meters are given by

$$L_{\text{outdoor-macro}}(d) = 8 + 37.6 \log_{10}(d), \tag{13}$$

$$L_{\text{pico-hotz}}(d) = 23.3 + 36.7 \log_{10}(d), \tag{14}$$

$$L_{\text{indoor}}(d) = L_{FS}(d) = 20 \log_{10}(4\pi d f_c/c), \text{for } d \leq d_{BP} \tag{15}$$

$$L_{\text{indoor}}(d) = L_{FS}(d_{BP}) + 35 \log_{10}(d/d_{BP}), \text{for } d > d_{BP} \tag{16}$$

where the break-point distances $d_{BP} = \{5, 5, 5, 10, 20, 30\}$ are for A...F models [24], correspondingly, and

$$L_{\text{D2D}}(d) = 58.6 \log_{10}(d) - 6.17, \tag{17}$$

where the attenuation is in decibels. The RF carrier frequency, f_c, is assumed to be 900 MHz, and c is the speed of light. For other center frequencies, f, a

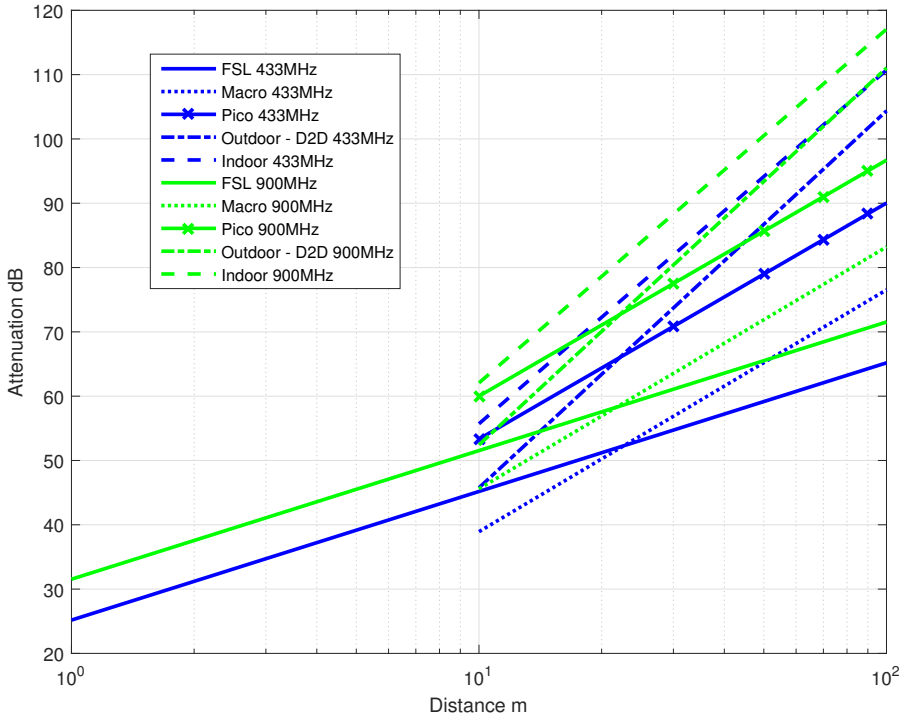

Fig. 2 Path losses for considered 802.11ah channels at 433 MHz and 900 MHz bands. Here $d_{BP} = 5$ for indoor channel. Free space loss, FSL, is also shown for reference

correction factor of $21\log_{10}(f/900\text{MHz})$ should be added. For completeness, the Free Space Loss attenuation [25] is given by

$$L_{\text{FSL}}(d) = 20\log_{10}(d) + 20\log_{10}(f_c) - 27.55. \tag{18}$$

Notice that even though the 802.11ah system itself is assumed to be deployed only at the 900 MHz (sub-1GHz) band, the above path loss models are indeed valid at other frequencies as well, as long as the proper correction factor stated above is applied.

In our numerical evaluations, we specifically focus on the licence-exempt ISM bands at 433 MHz and 900 MHz (sub-1GHz), due to their good suitability for low-power communications and being free from spectrum licencing related constraints. The principal path loss behaviors in the considered use cases versus the communication distance, d, are illustrated in Figure 2 at these two frequency bands. The path loss of indoor channel A shown in the figure, is the most demanding channel in path loss sense. Thus, this channel case will be considered in the continuation for path loss modeling.

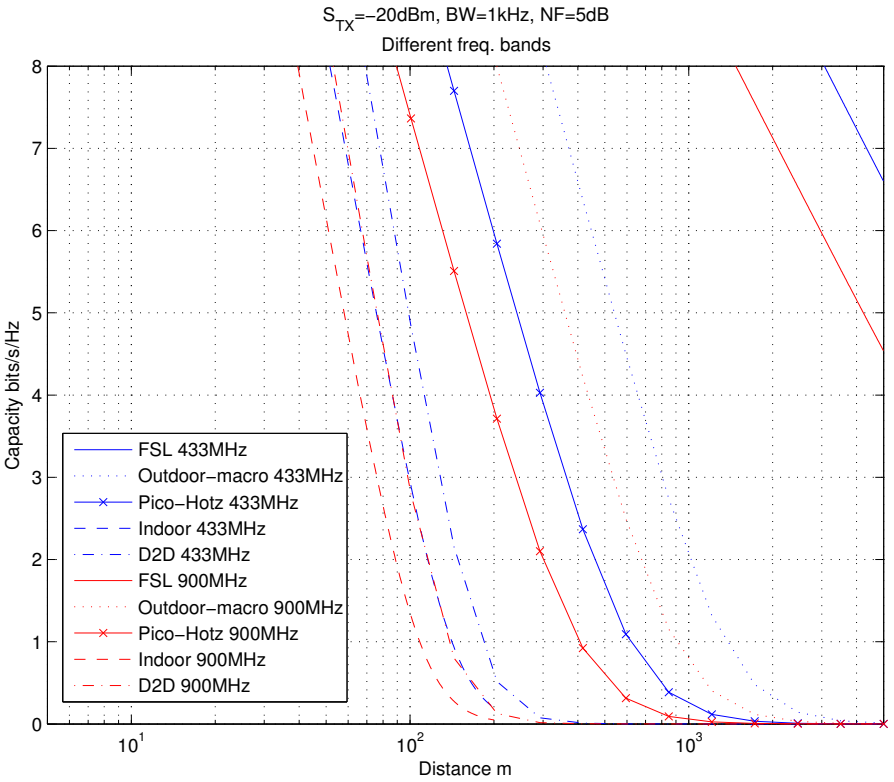

Fig. 3 Capacity wrt. distance in different channels at 433 MHz and 900 MHz. Here $d_{BP} = 5$ for indoor channel

4.2 Capacity Evaluations

In the following, the Shannon capacity in (4) will be evaluated in the limiting case when $\mu \to 1$, considering the different use cases and the two example ISM bands at 433 MHz and 900 MHz. Figure 3 shows the achievable capacity in bits/s/Hz, when the transmit power S_{TX} = -20 dBm, temperature $T = 290$K, bandwidth $B = 1$ kHz and the receiver NF = 5 dB. For example, in the outdoor D2D case at 433 MHz, the capacity bound is 4 bits/s/Hz (or 4 kbits/s with $B = 1$ kHz) at a distance of 112 meters. One can generally observe that the achievable capacity with the adopted realistic path loss models behaves very steeply versus the link distance. However, even with the considered very low transmit power of -20 dBm, outdoor link distances in the order of hundreds of meters can be achieved when the target spectral efficiency or capacity is in the realistic range of 1-5 bits/s/Hz. The low power levels proposed by the evaluations, imply also that zero-IF or direct conversion transceivers might be an option when considering the implementation of device. For completeness, the operational distances for all the listed channel scenarios, capacities 1 bit/s/Hz

Table 1
Achievable distances in meters for different bitrates and channel scenarios at 433 MHz / 900 MHz using 1 kHz bandwidth, and S_{TX}=-20 dBm.

Channel type	**Distance for 1 kbits/s 433 MHz / 900 MHz**	**Distance for 2 kbits/s 433 MHz / 900 MHz**
Indoor A	110 / 90	90 / 70
D2D	140 / 110	120 / 90
Pico-Hotz	450 / 290	330 / 220
Outdoor-macro	970 / 660	740 / 490

(1 kbits/s), 2 bits/s/Hz (2 kbits/s), for frequency bands 433 MHz, 900 MHz, and for 1 kHz bandwidth can be found in Table 1. Here again S_{TX}=-20 dBm.

Next, to understand better the range of needed transit powers in typical low-bit-rate sensor scenarios, we fix the required bitrate to 1 kbits/s together with an example bandwidth of 1 kHz, and use (4) to evaluate the required transmit power to reach the resulting capacity of 1 bit/s/Hz. The obtained results in terms of the required transmit powers at different link distances are shown in Figure 4. As can be seen, as a concrete example, the required transmit power level will be -28 dBm at 100 m distance for indoor channel case at 433 MHz. The corresponding value at 900 MHz will be -22 dBm. In general, depending on the environment, transmit powers even as low as -60 dBm can be sufficient to reach 1 bit/s/Hz capacity over a link distance of 100 m. This indicates that adopting low-rate IoT nodes without separate power amplifier (PA) module can be feasible, while still reaching link distances in the order of 100 m.

4.3 Achievable Operational Time

Next the achievable operational times using a capacitive energy storage with respect to transmit probability β_{TX} will be evaluated using (9). In all these evaluations, the target is to reach a bitrate of 1 kbit/s over a bandwidth of 1 kHz, i.e., the capacity is 1 bit/s/Hz, while the required link distance is fixed to 100 m. Furthermore, for simplicity, we consider only the indoor channel scenario, since it is the most challenging use case in terms of the path loss characteristics. For other channel scenarios the obtainable link distances are > 100 m.

Based on the results of the previous subsection (see Fig. 4), the required transmit powers for the considered communication scenario are S_{TX} = -28 dBm at 433 MHz and S_{TX} = -22 dBm at 900 MHz. Furthermore, we assume that the transmitter power efficiency $\alpha = 1/6.3 \approx 0.16$ (-8 dB), and thus the corresponding total transmitter power consumption values are P_{TX} = -20 dBm (433 MHz) and P_{TX} = -14 dBm (900 MHz). The energy storage supercapacitor characteristics are assumed to be similar as earlier, i.e., $U = 1$ V, $C_s = 0.5$

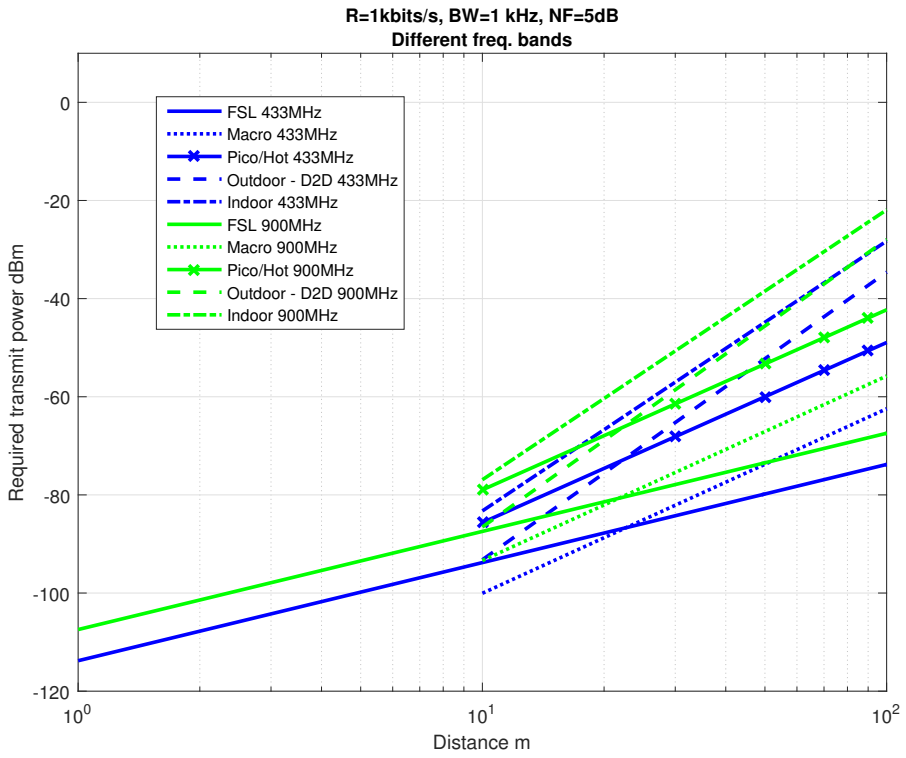

Fig. 4 Required transmit power vs. distance in different channels at 433 MHz and 900 MHz for $R = 1$ kbit/s and $B = 1$ kHz. Here $d_{BP} = 5$ for indoor channel

F, $\eta = 0.75$, and $I_l = 1$ μA. Finally, the ratio of power consumption of transmitter and receiver, ρ, is let to have different values between 0.1 and 10 in the evaluations to show the considered phenomena over large range of values.

The obtained results, when operating at 433 MHz, are shown in Figure 5. As was already shortly discussed in Subsection 3.3, when $\eta = 0.75$, $C_s = 0.5$ F, $U = 1$ V, $P_{TX} = 0.01$ mW, $\beta_{TX} = 0.01$, $\rho = 0.1$, and $I_l = 1$ μA, the achievable operation time $t_{op} \approx 25$ h. However, as can now be seen from the figure, if $\beta_{TX} = 0.1$ while still keeping $\rho = 0.1$, the operational time decreases to $t_{op} \approx 18$ h. Furthermore, if $\beta_{TX} \to 0$, meaning that the node is essentially only receiving, the maximum operational time saturates to $t_{op} \approx 26$ h, due to leakage current dominating the energy consumption.

Next also the required harvesting scenarios and needs are elaborated further. Coming back to the solar cell usage, discussed already shortly earlier in Subsection 3.3, it is possible to find the required size of the solar cell to satisfy the required overall transceiver energy consumption. By assuming similar harvesting intensities as in [23], namely 1 mW/cm^2, as well as the previous communication related constraints and energy consumption characteristics, the resulting size of the needed solar cell is shown in Figure 6. As can be seen,

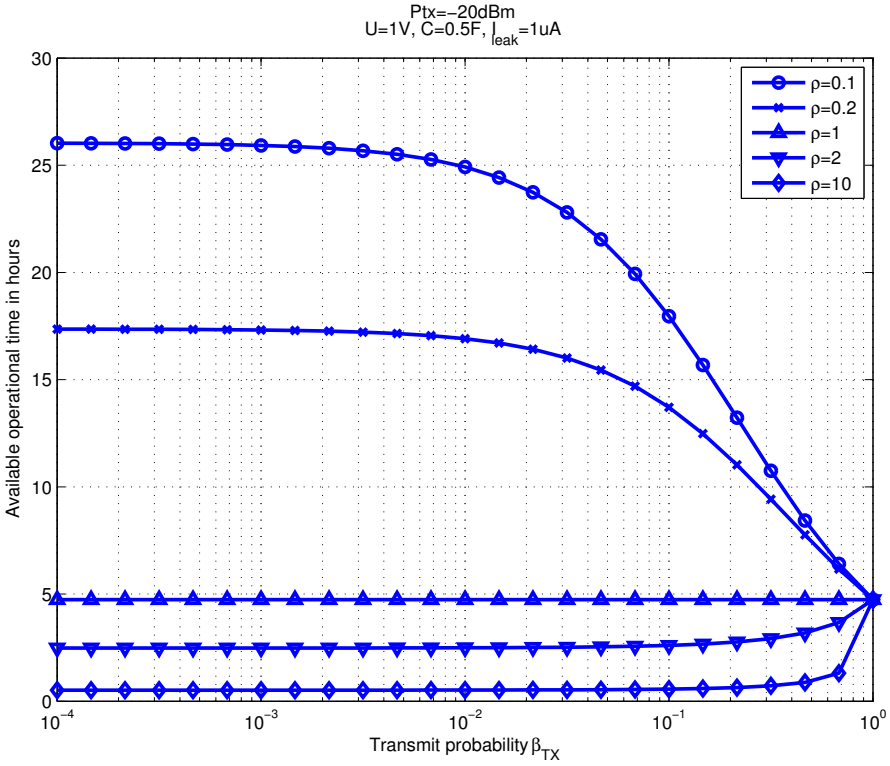

Fig. 5 Achievable operational time with respect to transmit probability β_{TX} for different values of ρ at 433 MHz band. The link distance is fixed at 100 m and capacity is 1 bit/s/Hz

for almost receive-only scenario, i.e., for very small values of β_{TX} and with $\rho = 0.1$, the required solar cell size is very small, that is 0.3 mm^2. Similarly for $\rho = 1$, the required solar cell area is 1.5 mm^2 while when $\rho = 10$, the required solar cell area is 13.5 mm^2, which is still quite small to be attached to, e.g., portable devices. Also with these relatively small solar cell areas, it might be possible to increase the size a little more and hence improve energy harvesting possibilities in unexpectedly varying lighting conditions. Then, when the transmit probability β_{TX} increases and hence β_{RX} decreases, the resulting solar cell size tends towards 1.5 mm^2. However, this case is somewhat artificial since typically it is expected that the transceiver is not operating in transmitter mode very frequently. If the lighting conditions change more, e.g., the lighting intensity decreases by one order of magnitude, also the energy harvesting needs change accordingly, so that the transceiver is still supplied by the same amount of energy. In such cases, the needed solar cell size will also increase accordingly.

Next, similar evaluations are carried out also at the 900 MHz band assuming similar energy harvesting and storage capabilities. Due to the larger path loss attenuation compared to the previous 433 MHz case, the transmit power

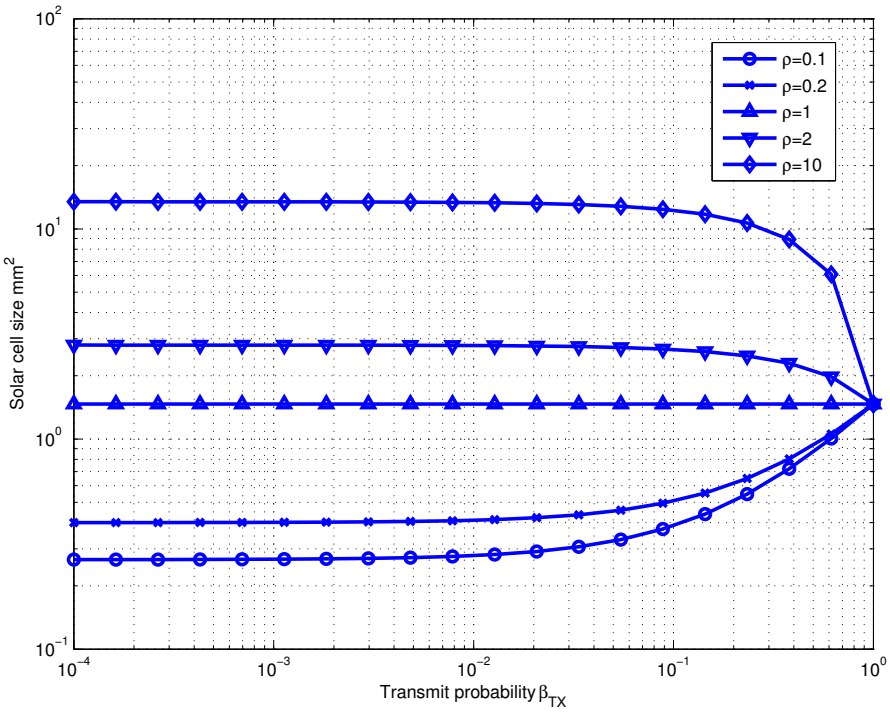

Fig. 6 Required solar cell area with respect to transmit probability β_{TX} for different values of ρ at 433 MHz band

needs to be increased now to -22 dBm to reach the 100 m communication distance in the worst case indoor channel at rate 1 bit/s/Hz. With the assumed transmitter power efficiency corresponding to an 8 dB implementation loss, the total consumed power will thus be -14 dBm. This is then clearly reflected in the achievable operational time as can be seen in Figure 7. As the figure illustrates, now only about half of the operational time at 433 MHz band can be achieved. Also the requirements for the solar cell area are clearly increased as can be seen in Figure 8, with the required area being roughly fourfold in comparison to the previous 433 MHz band case.

Lastly, in Figure 9 the allowed maximum leakage current (8) is illustrated with respect to transmit probability, β_{TX}, for the selected values of the ratio of the receiver and transmitter power consumption, ρ. In this example solar cell size of 9 mm^2 is assumed, while the other parameters are the kept as defined earlier. The cases of targeted total transmitter power consumption values P_{TX} = -20 dBm (433 MHz) and P_{TX} = -14 dBm (900 MHz) are again considered. If the supercapacitor leakage current is not below these values, no supercapacitor recharging may take place. However with smaller leakage current values, recharging occurs. As may be seen at 900 MHz and for $\rho = 3$, the recharging will only be possible when $\beta_{TX} \geq 0.4$.

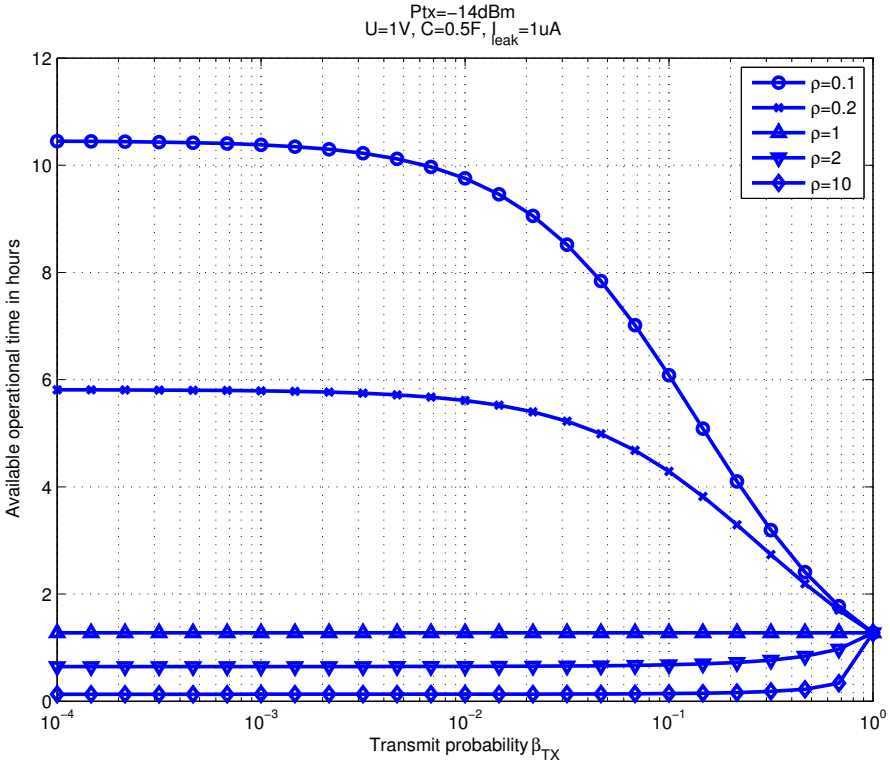

Fig. 7 Achievable operational time with respect to transmit probability β_{TX} for different values of ρ at 900 MHz band. The link distance is fixed at 100 m and capacity is 1 bit/s/Hz

5 Conclusion

In this paper, the feasibility and fundamental limits of energy harvesting based M2M communications were studied and evaluated. The theoretical bounds essentially based on Shannon theorem combined with elementary propagation models, implementation losses and the amount of available energy were established and evaluated. Furthermore, expressions for the achievable communication time were established depending on the amount of harvested energy and its storage capabilities as well as the assumed probabilities to transmit and receive over the considered time window. As concrete examples, a supercapacitor was adopted as an energy storage while the energy harvesting was assumed to be building on a tiny economical solar cell. Large set of numerical results were also reported, specifically at the licence-exempt ISM bands at 433 MHz and 900 MHz (sub-1GHz), while the analysis methodology and derived expressions are generally valid at other frequencies as well. The provided analysis methodology and obtained results establish clear feasibility regions and performance bounds for energy harvesting based low-rate M2M communications in the future IoT networks.

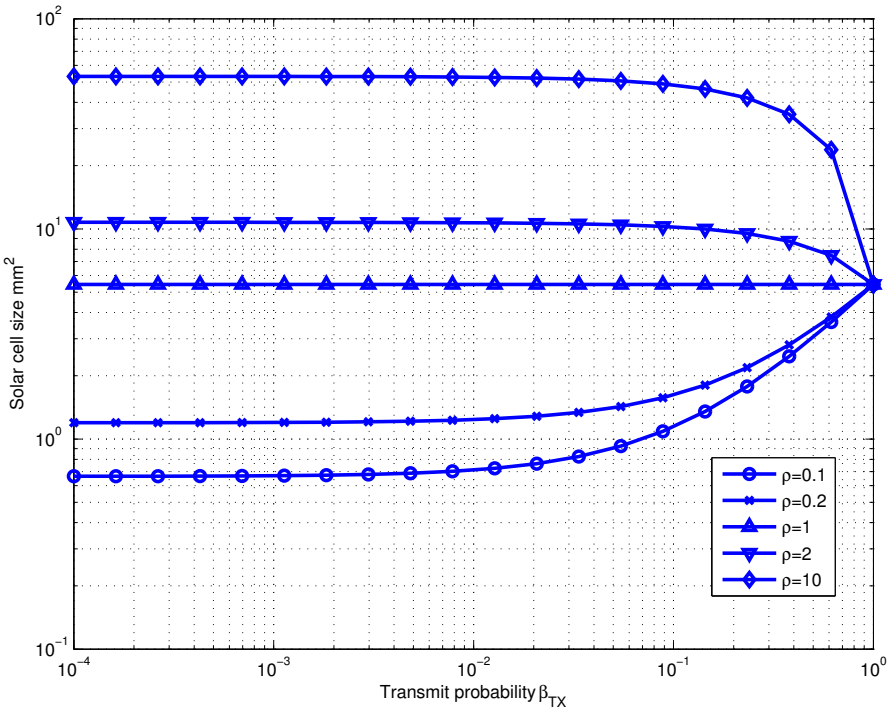

Fig. 8 Required solar cell area with respect to transmit probability β_{TX} for different values of ρ at 900 MHz band

References

1. J. Rinne *et al.*, "Feasibility and Fundamental Limits of Energy-Harvesting Based M2M Communications," in *Proc. IEEE 27th Annual International Symposium on Personal, Indoor, and Mobile Radio Communications (PIMRC)*, pp. 318-323, Sept. 2016.
2. Ericsson, Mobility report, Nov. 2016. Available [online] at https://www.ericsson.com/assets/local/mobility-report/documents/2016/ericsson-mobility-report-november-2016.pdf
3. S. Andreev *et al.*, "Understanding the IoT Connectivity Landscape: A Contemporary M2M Radio Technology Roadmap," *IEEE Comm. Mag. Communications Standards Supplement*, vol. 53, no. 9, pp. 32-40, Sept. 2015.
4. V. Raghunathan *et al.*, "Energy aware wireless microsensor networks," *IEEE Signal Process. Mag.*, vol. 19, no. 2, pp. 40-50, Mar. 2002.
5. S. Sudevalayam *et al.*, "Energy harvesting sensor nodes: Survey and implications," *IEEE Commun. Surveys Tuts.*, vol. 13, no. 3, pp. 443-461, 3rd Quart. 2011.
6. X. Chen *et al.*, "Low power sensor design for IoT and mobile healthcare applications," *China Communications*, vol. 12, no. 5, pp. 42-54, May 2015.
7. S. Ulukus *et al.*, "Energy Harvesting Wireless Communications: A Review of Recent Advances," *IEEE Journal on Selected Areas in Communications*, vol. 33, no. 3, pp. 360-381, March 2015.
8. S. Lehtimaki *et al.*, "Low-cost solution processable carbon nanotube-based supercapacitors and their characterization," *Appl. Phys. A*, 2014.
9. G. Nisato *et al.*, *Organic and Printed Electronics: Fundamentals and Applications*, Pan Stanford, 2016.

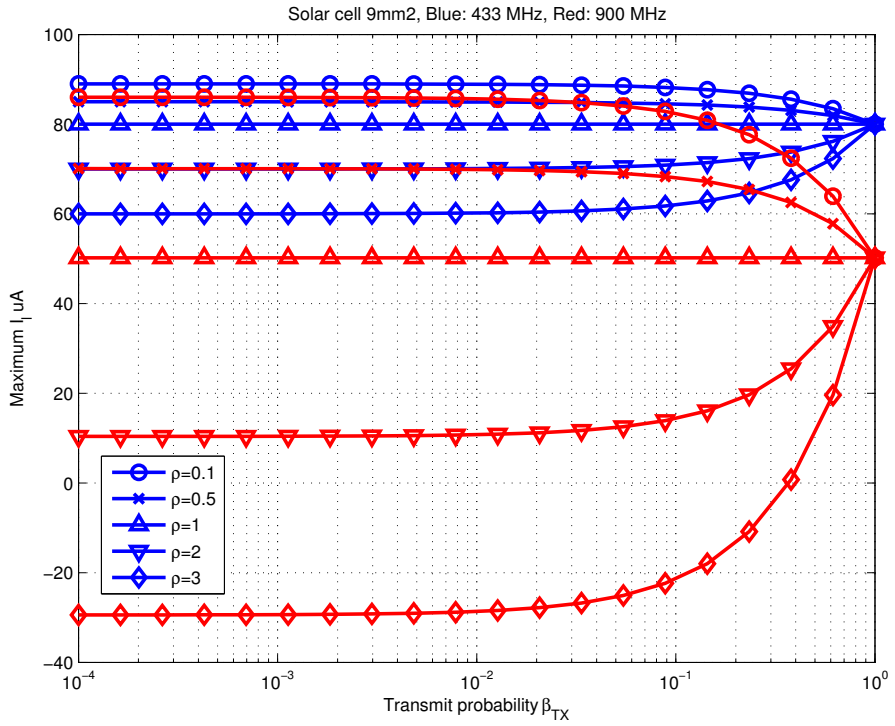

Fig. 9 Allowed maximum leakage current with respect to transmit probability β_{TX} for different values of ρ at different bands. Blue: 433 MHz band ($P_{TX} = -20$ dBm), Red: 900 MHz band ($P_{TX} = -14$ dBm)

10. J. Keskinen *et al.*, "Architectural modifications for flexible supercapacitor performance optimization," *Electronic Materials Letters*, DOI: 10.1007/s13391-016-6141-y, 2016.
11. S. Lehtimaki *et al.*, "Performance of printable supercapacitors in an RF energy harvesting circuit," *Int. Journal of Electrical Power and Energy Systems*, vol. 58, pp. 42-46, 2014.
12. C. E. Shannon, "A mathematical theory of communication," *ACM SIGMOBILE Mobile Computing and Communications Review*, vol. 5, no. 1, pp. 3-55, Reprinted (with corrections from Shannon 1948), 2001.
13. Rec. ITU-R P.372-12, "Radio Noise," ITU-R Geneva, July 2015.
14. J. G. Proakis, *Digital Communications*, 4th ed., McGraw-Hill, 2000.
15. S. ten Brink, "A rate one-half code for approaching the Shannon limit by 0.1dB," *IEE Electronics Letters*, vol. 36, no. 15, pp. 1293-1294, July 2000.
16. F. K. Shaikh *et al.*, "Energy harvesting in wireless sensor networks: A comprehensive review," *Renewable and Sustainable Energy Reviews* 55, pp. 1041-1054, 2016.
17. G. Tuna *et al.*, "Energy harvesting and battery technologies for powering wireless sensor networks," *Industrial Wireless Sensor Networks: Monitoring, Control and Automation*, pp. 25-38, 2016. doi:10.1016/B978-1-78242-230-3.00002-7.
18. D. Niyato *et al.*, "Wireless sensor networks with energy harvesting technologies: A game-theoretic approach to optimal energy management," *IEEE Wireless Communications*, vol. 14, no. 4, pp. 90-96, 2007.
19. J. A. Paradiso *et al.*, "Energy scavenging for mobile and wireless electronics," *IEEE Pervasive Comput.*, vol. 4, no. 1, pp. 18-27, Jan.-Mar. 2005.
20. J. Bird, *Electrical and Electronic Principles and Technology*, Routledge, 2010.

21. L. Gu *et al*, "Radio-triggered wake-up for wireless sensor networks," *Real-Time Sys.*, vol. 29, no. 2, pp. 157-182, 2005.
22. J. Ansari *et al.*, "Radio-triggered wake-ups with addressing capabilities for extremely low power sensor network applications," *Int J. Wireless Inf Networks*, vol. 16, no. 3, pp. 118-130, July 2009.
23. M. T. Penella-Lopez and M. Gasulla, *Powering Autonomous Sensors: An Integral Approach with Focus on Solar and RF Energy Harvesting*, 1st ed., Springer, 2011.
24. IEEE P802.11 Wireless LANs TGah Channel Model, (doc.: IEEE 802.11-11/0968r4), March 2015.
25. Rec. ITU-R P.525, "Calculation of free-space attenuation," ITU-R Geneva, Aug. 2003.